

Importance of Elevation and Temperature Inversions for the Interpretation of Thermal Infrared Satellite Images Used in Geothermal Exploration

Mariana Eneva¹ and Mark Coolbaugh²

¹Imageair, Inc., San Diego, CA, meneva@imageair-inc.com

²Great Basin Center for Geothermal Energy, University of Nevada, Reno, NV, sereno@dim.com

Keywords

Thermal infrared, TIR, geothermal exploration, ASTER, temperature inversions, Coso geothermal field

ABSTRACT

Examples of nighttime temperature inversions are shown in thermal infrared satellite images collected over the Coso geothermal field in eastern California. Temperature-elevation plots show the normal trend of temperature decrease with elevation, on which temperature inversions appear superimposed as opposite trends. Such inversions are common and they should be taken into account, along with the elevation effects, in order to optimize the correct identification in satellite images of surface temperature anomalies associated with geothermal systems.

Background

In an effort to aid geothermal exploration, satellite imagery from the Advanced Spaceborne Thermal Emission and Reflection Radiometer (ASTER) has been used to look for surface expressions of temperature anomalies possibly associated with geothermal fields (Coolbaugh et al., 2007; Eneva et al., 2006, 2007). ASTER is a Japanese instrument mounted on the U.S. Terra satellite that provides multispectral images in 14 channels: three visible and near-infrared (VNIR) with 15-m resolution; six short-wave infrared (SWIR) with 30-m resolution; and five thermal infrared (TIR) channels (8 to 12 μm wavelengths) with 90-m resolution. The multichannel ASTER TIR is used to obtain emissivity and surface temperature imagery products by applying a temperature-emissivity separation (TES) algorithm (e.g., Gillespie et al., 1998). Of particular importance for our applications has been the AST_08 product, which is an image of kinetic surface temperature. Reflection products (AST_07 and AST_07XT) were also used for the purpose of applying albedo corrections to the AST_08 products. Unlike the reflection products, AST_08 are available for both day- and nighttime imagery.

Coolbaugh et al. (2007) have demonstrated that the ability of AST_08 products to detect temperature anomalies can be improved if corrections are applied for factors such as albedo, topographic slope aspect, and thermal inertia. For example, southern slopes are warmer than northern slopes in the northern hemisphere, an effect that although much stronger during the day, can endure during the night, yet has nothing to do with the possible presence of temperature anomalies due to subsurface processes. Coolbaugh et al. (2007) reported examples from Nevada, where the corrected AST_08 products showed temperature anomalies that were not evident in the uncorrected images. Eneva et al. (2006, 2007) applied these same methods in eastern California.

However, the effect of topography on the AST_08 products is not limited to the effect of the topographic slope aspect on surface temperature. Other factors include elevation and temperature inversions that ideally should be removed before searching for temperature anomalies (Quattrochi et al., 2009). Here examples derived from AST_08 imagery are shown, collected over the Coso geothermal field in August 2006.

Effect of Elevation

With all other factors equal, both air and surface temperatures generally decrease as the elevation increases. This effect is more readily discernable at night. During the day high temperature contrasts between sunlit and shaded areas can significantly distort the effect of elevation. Therefore, it is likely best to correct for the elevation effect after the effects of albedo and topographic slope aspect are removed. A theoretical adiabatic lapse rate of -9.8°C per 1 km of elevation is cited in the meteorological literature (e.g., Chapman et al., 2001). The so-called “environmental” lapse rate generally observed in nature is lower, due mostly to the presence of water vapor, with $-6.5^{\circ}\text{C}/\text{km}$ assumed to be suitable in most cases. The temperature-elevation trend can be so pronounced in some cases that it has been possible to effectively use it as a surrogate to calculate missing data in digital elevation models (Crippen et al., 2007).

Figures 1 to 4 show temperature-elevation plots from Coso in eastern California, in which the decrease of surface temperature with elevation is a dominant trend. The surface temperatures are taken from AST_08 with spatial resolution of 90 m, while the elevations are from USGS digital elevation models (DEM) with spatial resolution of 30 m (downloaded from <http://seamless.usgs.gov>). Nighttime and daytime AST_08 covering the same area are used in Figures 1 and 2, respectively. The nighttime lapse rate of about $-5^{\circ}/\text{km}$ indicated by the slope of the straight line in Figure 1 is lower than the expected

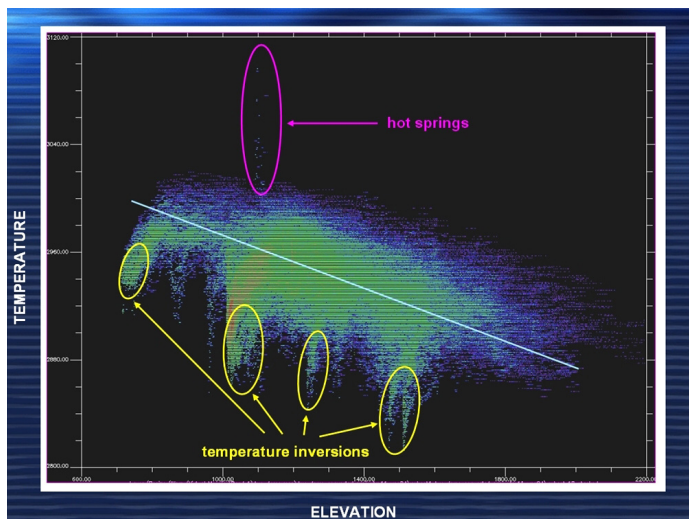


Figure 1. Nighttime density plot of surface temperature versus elevation extracted from a nighttime ASTER TIR image. Temperature inversions (yellow outlines) are superimposed on the normal temperature decrease with elevation (average trend is approximated by the light blue straight line). Hot springs and fumaroles have a distinct range of high temperatures not dependent on elevation (pink outline).

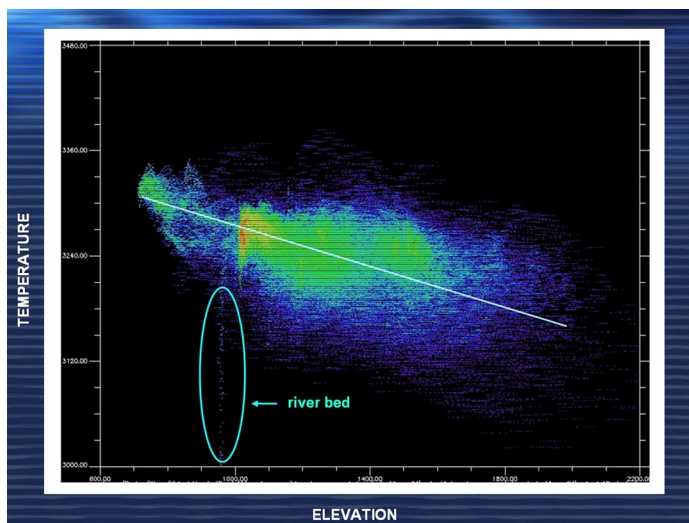


Figure 2. Daytime density plot of surface temperature versus elevation extracted from a daytime ASTER TIR image covering the same area as in Figure 1. Normal temperature decrease with elevation (average trend is approximated by light blue straight line) is not contaminated by temperature inversions. Hot springs are not evident either. A river valley is represented by a range of low temperatures not dependent on elevation.

environmental lapse rate of $-6.5^{\circ}/\text{km}$ (e.g., Crippen et al., 2007), likely due to temperature inversions (discussed below) superimposed on the usual temperature-elevation trend. Away from temperature inversions spatially varying lapse rates were obtained between $-5.4^{\circ}/\text{km}$ and as high as $-9.8^{\circ}/\text{km}$, which is the adiabatic lapse rate.

Figure 2 shows a similar plot, but surface temperatures are taken from the daytime AST_08. In this case the average lapse rate over the whole area represented by the slope of the straight line was found to be $-8.4^{\circ}/\text{km}$. However, due to high contrasts in solar irradiation for some portions of the area covered by AST_08, some very steep temperature-elevation relationships were observed, with slopes up to $-30^{\circ}/\text{km}$. This underlines the necessity to eliminate the differential effects of slope and aspect before attempting to derive credible lapse rates from daytime TIR imagery. It is to be noted that unlike in the nighttime, the daytime temperature-elevation relationship is not contaminated by temperature inversions.

Effect of Temperature Inversions

The normal effect of elevation on surface temperature can be reversed due to the meteorological phenomenon of temperature inversions (e.g., Chapman et al., 2001), more frequently observed at night and in the winter. In relatively stable atmospheric conditions (i.e., low wind speed), a layer of cold air can form close to the surface that gets pulled by gravity, moving downward through drainage channels (so-called katabatic flow) until topographic or meteorological barriers are reached. As a result, the bottoms of valleys may become colder compared with higher elevations and thus temperature inversions take place. The increase of temperature with elevation may stop at the foot of hills and mountains, above which the normal decrease of temperature with elevation resumes. This may lead to formation of relatively warm belts at the base of mountains. Temperature inversions can be sustained only at

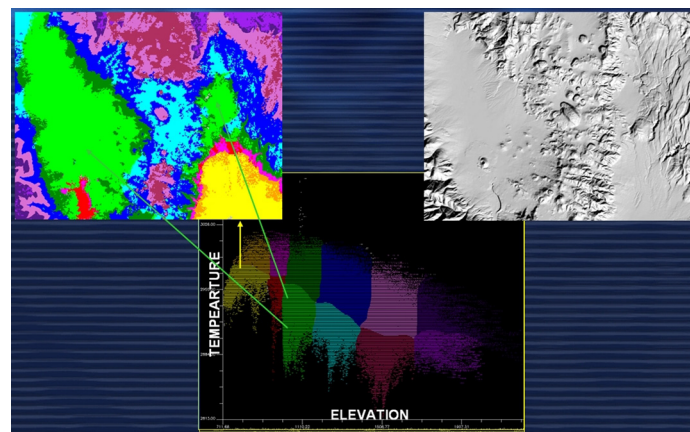


Figure 3. Map representation of the nighttime temperature inversions. Temperature-elevation plot is same as in Figure 1, but divided in color sections to identify corresponding areas on map. Inset in the top right shows map of shaded relief in the area of the Coso geothermal field. Inset in the top left shows the same map but with color coded temperatures from a nighttime ASTER TIR image, with temperatures increasing from blue to red.

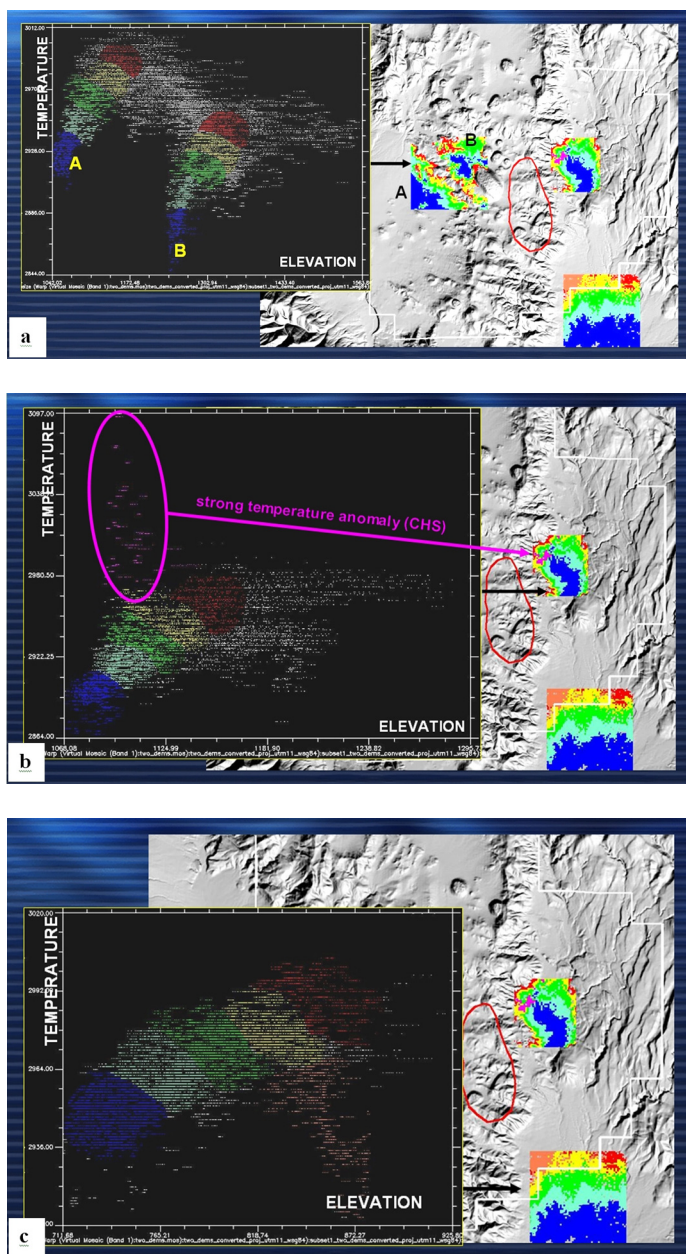


Figure 4. Examples of nighttime temperature inversions from ASTER TIR imagery. Inset to the right shows a map of shaded relief at the Coso geothermal field (same as in Figure 3). White outline marks the KGRA (known geothermal resource area). Red outline marks the production area. Rectangles with color denote three areas with distinct nighttime inversions. Colors in rectangles show increasing temperatures from blue to red. Inset to the left shows temperature-elevation plots, with the colored areas corresponding to the colors from the map of shaded relief. (a) An area east and north-east from Sugar Mountain. Note two distinct branches A and B superimposed on normal decrease of temperature with elevation. These temperature inversions developed on both sides of a ridge as seen from the map. (b) An area including the Coso Hot Springs (CHS) marked by pink color for the highest temperatures (also seen in Figure 1). (c) A valley in the south-eastern corner of the map.

lower wind speeds, and if the winds are stronger, they do not form. Thus the same areas may exhibit such inversions on some nights, but not on others.

Figures 1, 3, and 4 illustrate these effects, as derived from nighttime AST_08. Such inversions are possible during the day as well, but mostly in winter. The AST_08 images used here are from the summer (month of August), so the daytime AST_08 does not show the presence of temperature inversions (Figure 2).

Figure 1 shows several temperature inversions superimposed on the normal temperature-elevation trend. It also shows hot springs appearing in this type of representation as a wide range of high surface temperatures at a constant elevation. One can envision using such quick temperature-elevation plots in a search for hot springs in nighttime TIR images over isolated and difficult-to-access areas. Such plots may be also helpful even if geothermal temperature anomalies are more subtle, but the effects of albedo and topographic slope aspect would have to be removed, in order to reduce the scatter seen in Figure 1.

The temperature-elevation scatter plot shown in Figure 3 is the same as that in Figure 1, however different parts are colored with the same colors as the areas in a map that correspond to these parts of the plot. It is evident that certain portions of the plot, including the temperature inversion branches, correspond to spatially coherent areas in the map rather than being spatially scattered throughout the image.

Three examples of individual sub-areas with nighttime temperature inversions are shown in Figure 4. Note the two distinct inverted branches A and B coming prominently out of a normal temperature-elevation trend (Figure 4a), corresponding to areas on both sides of a ridge. The same hot spring anomaly seen in the more generalized plot in Figure 1 is easily attributable here to the Coso Hot Springs area (Figure 4b). The third example is from a part of the area with the lowest elevations, where a valley transitions into higher elevations (Figure 4c).

Conclusions

It was demonstrated that nighttime temperature inversions are common rather than rare. It is thus imperative that they are taken into account, along with the effects of elevation, when satellite thermal infrared imagery is used to search for surface temperature anomalies attributable to subsurface processes, such as geothermal activity.

Acknowledgements

This study is part of a research project funded by the California Energy Commission (CEC) with PIER Grant PIR-04-006.

References

- Chapman, L., J.E. Thornes, and A.V. Bradley, 2001. Statistical modeling of road surface temperature from a geographical parameter database, *Meteorological Applications* **8**, p. 409-419.
- Coolbaugh, M.F., C. Kratt, A. Fallacaro, W.M. Calvin, and J.V. Taranik, 2007. Detection of geothermal anomalies using Advanced Spaceborne Thermal Emission and Reflection Radiometer (ASTER) thermal infrared images at Brady's Hot Springs, Nevada, USA, *Remote Sensing of Environment* **106**, p. 350-359.

- Crippen, R.E., S.J. Hook, and E. Fielding, 2007. Nighttime ASTER thermal imagery as an elevation surrogate for filling SRTM DEM voids, *Geophys. Res. Lett.* **34**, doi:0.1029/2006GL028496.
- Eneva, M., M. Coolbaugh, S. Bjornstad, and J. Combs, Detection of surface temperature anomalies in the Coso geothermal field using thermal infrared remote sensing, 2007. *Geothermal Resources Council Transactions* **31**, p. 335-340.
- Eneva, M., M. Coolbaugh, and J. Combs, 2006. Application of satellite thermal infrared imagery for geothermal exploration in east central California, *Geothermal Resources Council Transaction* **30**, p. 407-411.
- Gillespie, A., S. Rokugawa, T. Matsunaga, J. S. Cothorn, S. J. Hook, and A. Kahle, 1998. A Temperature and Emissivity Separation Algorithm for Advanced Spaceborne Thermal Emission and Reflectance Radiometer (ASTER) Images, *IEEE Trans. Geosci. Rem. Sens.* **36**, p. 1113-1126.
- Quattrochi, D.A., A. Prakash, M. Eneva, R. Wright, D.K. Hall, M. Anderson, W.P. Kustas, R.G. Allen, T. Pagano, M.F. Coolbaugh, 2009. Thermal Remote Sensing: Theory, Sensors, and Applications, Chapter 3 in *Manual of Remote Sensing*, 4th Edition, American Society of Photogrammetry and Remote Sensing, Falls Church, VA. (in press).